NANO · MICRO small
www.small-journal.com

Polymeric Nanoparticles with Neglectable Protein Corona

Irina Alberg, Stefan Kramer, Meike Schinnerer, Qizhi Hu, Christine Seidl, Christian Leps, Natascha Drude, Diana Möckel, Cristianne Rijcken, Twan Lammers, Mustafa Diken, Michael Maskos, Svenja Morsbach, Katharina Landfester, Stefan Tenzer, Matthias Barz,* and Rudolf Zentel**

The current understanding of nanoparticle–protein interactions indicates that they rapidly adsorb proteins upon introduction into a living organism. The formed protein corona determines thereafter identity and fate of nanoparticles in the body. The present study evaluates the protein affinity of three core-crosslinked polymeric nanoparticles with long circulation times, differing in the hydrophilic polymer material forming the particle surface, namely poly(*N*-2-hydroxypropylmethacrylamide) (pHPMA), polysarcosine (pSar), and poly(ethylene glycol) (PEG). This includes the nanotherapeutic CPC634, which is currently in clinical phase II evaluation. To investigate possible protein corona formation, the nanoparticles are incubated in human blood plasma and separated by asymmetrical flow field-flow fractionation (AF4). Notably, light scattering shows no detectable differences in particle size or polydispersity upon incubation with plasma for all nanoparticles, while in gel electrophoresis, minor amounts of proteins can be detected in the particle fraction. Label-free quantitative proteomics is additionally applied to analyze and quantify the composition of the proteins. It proves that some proteins are enriched, but their concentration is significantly less than one protein per particle. Thus, most of the nanoparticles are not associated with any proteins. Therefore, this work underlines that polymeric nanoparticles can be synthesized, for which a protein corona formation does not take place.

1. Introduction

In the last decades, nanosized carrier systems for pharmaceutically active compounds have not only attracted the attention of researchers worldwide, but also emerged into clinical trials or even became approved drugs.[1–3] Many attempts have been made to modify the biodistribution toward higher target site accumulation, which requires engineering nanoparticle properties, e.g., size and surface.[4] In this context, the potential formation of a protein corona around nanoparticles is of primary interest, since this process changes the nanoparticle surface properties and thus co-determines the biological profile in the body.[5–7]

Protein corona formation of various nanoparticles and its impact on pharmacokinetics has been carefully studied.[8–10] The tested nanoparticles were mainly inorganic or organic colloidal nanoparticles,[11–14] for which a pronounced corona formation was observed upon contact with plasma proteins. This protein corona modifies the interaction

I. Alberg, Dr. S. Kramer, C. Seidl, Prof. M. Barz, Prof. R. Zentel
Institute of Organic Chemistry
Johannes Gutenberg University Mainz
Duesbergweg 10-14, Mainz D-55128, Germany
E-mail: zentel@uni-mainz.de; barz@uni-mainz.de

Dr. M. Schinnerer
Institute of Physical Chemistry
Johannes Gutenberg University Mainz
Duesbergweg 10-14, Mainz D-55128, Germany

Dr. Q. Hu, Dr. C. Rijcken
Cristal Therapeutics
Oxfordlaan 55, Maastricht 6229 EV, The Netherlands

The ORCID identification number(s) for the author(s) of this article can be found under https://doi.org/10.1002/smll.201907574.

© 2020 The Authors. Published by WILEY-VCH Verlag GmbH & Co. KGaA, Weinheim. This is an open access article under the terms of the Creative Commons Attribution-NonCommercial License, which permits use, distribution and reproduction in any medium, provided the original work is properly cited and is not used for commercial purposes.

DOI: 10.1002/smll.201907574

C. Leps, Prof. S. Tenzer
Institute for Immunology
University Medical Center of Mainz
Langenbeckstr. 1, Mainz 55131, Germany
E-mail: tenzer@uni-mainz.de

N. Drude, D. Möckel, Prof. T. Lammers
Department of Nanomedicine and Theranostics
Institute for Experimental Molecular Imaging
RWTH Aachen University Clinic
Forckenbecktrasse 55, Aachen 52074, Germany

Dr. M. Diken
TRON - Translational Oncology at the University Medical Center of Johannes Gutenberg University gGmbH
Freiligrathstr. 12, Mainz 55131, Germany

Prof. M. Maskos
Fraunhofer Institute for Microengineering and Microsystems IMM
Carl-Zeiss-Str. 18-20, Mainz 55129, Germany

Prof. S. Morsbach, Prof. K. Landfester
Max Planck Institute for Polymer Research
Ackermannweg 10, Mainz 55128, Germany

 © 2020 The Authors. Published by WILEY-VCH Verlag GmbH & Co. KGaA, Weinheim

with cells,[10] can shield recognition units,[15] but its role for biodistribution and circulation is still far from well understood.[8,16]

Except for liposomes, other types of nano-sized drug delivery systems, such as polymeric micelles or more complex polymer constructs like cylindrical polymer brushes[17] have been so far hardly investigated with respect to protein corona formation (for comparison between the structures of these nanoparticles and the colloidal nanoparticles discussed above, see Figures S1 and S2 in the Supporting Information).[8,18–20] However, the former are interesting, since polymeric micelles are in advanced stages of clinical testing (e.g., CPC634 (phase II)[21] and NC-6004 Nanoplatin (phase III)[22]).

To evaluate the formation of a protein corona, separation of the nanoparticle–protein-complex from unbound proteins used for incubation or upon in vivo exposure becomes a necessity. The isolation of incubated nanoparticles (colloids and inorganic nanoparticles) from unbound proteins was mainly performed by centrifugation, which is a separation method based on differences in density.[23] Thus, this method allows only the purification of nanoparticles with a higher density but can hardly be used for low density particles, such as polymeric micelles and polymer brushes.[24] Only recently, size exclusion techniques such as size exclusion chromatography and asymmetrical flow field-flow fractionation (AF4) have been employed for this purpose.[19,25,26] AF4 is a separation technique, which can be applied for the separation of particle and protein mixtures in the size range between 1 nm and 1 µm.[27,28] It consists of a separation channel with a flow gradient in which the particles are separated by an additional vertical force field depending on their diffusion coefficient.[29,30] During an AF4 measurement, the injected particles are pushed by the vertical cross flow toward the membrane at the bottom of the channel. Due to Brownian motion, the particles are diffusing back into the middle of the channel. Since smaller particles are faster than larger ones (because of their higher diffusion coefficient), they are concentrating faster in the middle, thus eluting first through the channel outlet. In contrast to conventional size exclusion chromatography, in AF4 the contact to the interface and the shear forces are substantially reduced, which leads to very mild separation conditions, minimizing perturbations of a potential protein corona.[26,31] Based on this method, Landfester and coworkers recently fully characterized the protein corona of Lutensol AT50-coated polystyrene nanoparticles and PEG functionalized liposomes, identifying all adsorbed proteins.[19,26]

Here, we present a purification procedure based on AF4 for the separation of smaller polymeric architectures (R_h: 20–30 nm) that are hardly separable by centrifugation. We isolated polymeric nanoparticles from unbound blood plasma components and characterized them by dynamic light scattering, gel electrophoresis and mass spectrometry, with the goal of studying their protein corona and their affinity to specific plasma proteins. As model systems we selected polymer micelles and a molecular polymer brush, which are close to established nanocarriers concerning their hydrophilic shell (see **Figure 1**). As shell material we chose either i) poly(ethylene glycol) (PEG),[25,32] ii) poly(*N*-2-hydroxypropylmethacrylamide) (pHPMA)[18,33,34] or iii) polysarcosine (pSar),[35,36] as they are not only considered protein resistant but furthermore are part of drugs in preclinical or clinical investigations.[21,37–39] Moreover, all these polymers are hydrophilic and do not possess a net charge to reduce adsorption of proteins by electrostatic and hydrophobic interactions.[40,41] In addition, it was recently demonstrated that the pSar based nanoparticles maintain their diffusion coefficient and thus hydrodynamic radius even in full human blood.[42] From the chemical side PEG and pSar follow the Whitesides Rules for protein resistant materials, as they are hydrophilic and only weak H-bond acceptors without a net charge and H-bond donor properties.[43] Moreover, pSar and PEG possess identical solution properties in aqueous solution.[44] pHPMA, however, possesses H-bond donor-properties (amide and hydroxyl proton). Nevertheless, pHPMA homopolymers of 65 kDa display a blood half-life of 10 h.[45] Generally, surface coatings with these polymers reduce protein adsorption.[43,46] In this context, the interactions between PEG and pSar were investigated using molecular dynamic simulations, where only minimal protein interactions were found.[47]

Here we want to use the AF4 technique, for a comparative analysis of three micellar carrier systems to determine their protein corona.

2. Results and Discussion

For this study we selected three polymer-based nanoparticles (see Figure 1), which have a surface either based on PEG, pSar or pHPMA. Physicochemically, all selected nanoparticles resemble core-crosslinked polymeric micelles although they were synthesized in rather different ways (see Figure S1 in the Supporting Information). These are two polymer micelles based on amphiphilic block copolymers with poly(*N*-2-hydroxypropylmethacrylamide) (pHPMA-NP)[48] or poly(ethylene glycol) (PEG-NP)[32] as the hydrophilic block and they are crosslinked in the hydrophobic block after self-assembly (see Figure S1 in the Supporting Information). The third system is a polymer brush with a hydrophobic *N*-acylated poly(lysine) main chain and a hydrophilic poly(sarcosine) shell (pSar-NP) (Figure S1, Supporting Information).[49] These three nanoparticles were synthesized according to the published protocols.[32,48,49] It is important to state that the presented nanoparticles differ in chemistry, but share a common feature, which is the covalent stabilization of the core to assure stability after injection into a living species.[17] In fact, all systems represent single large molecules, in case of PEG- and pHPMA-NPs with a core shell structure, in which the exchange dynamics between micelles and unimers are abolished. Consequently, all three systems can be regarded as stable nanoparticles with a dense, hydrophilic polymer shell even in contact with plasma proteins or cell membranes.

All nanoparticles were characterized by multiangle laser light scattering in aqueous solution ensuring that the particles are of comparable size. They are in a size range of R_h = 20–30 nm and display a polydispersity (µ2) of below 0.11, indicating nanoparticles with narrow size distribution. In addition, all three systems reveal a ζ-potential between –7 and –0.1 mV, which is considered as neutral charge for nanoparticles.[50] Data on size distribution and ζ-potential of the individual particles are shown in Figure 1 and Figures S3–S5 in the Supporting Information. Thus, these nanoparticles fulfill the preconditions for a good in vivo circulation,[40] which was verified in Figure 1a–d.

© 2020 The Authors. Published by WILEY-VCH Verlag GmbH & Co. KGaA, Weinheim

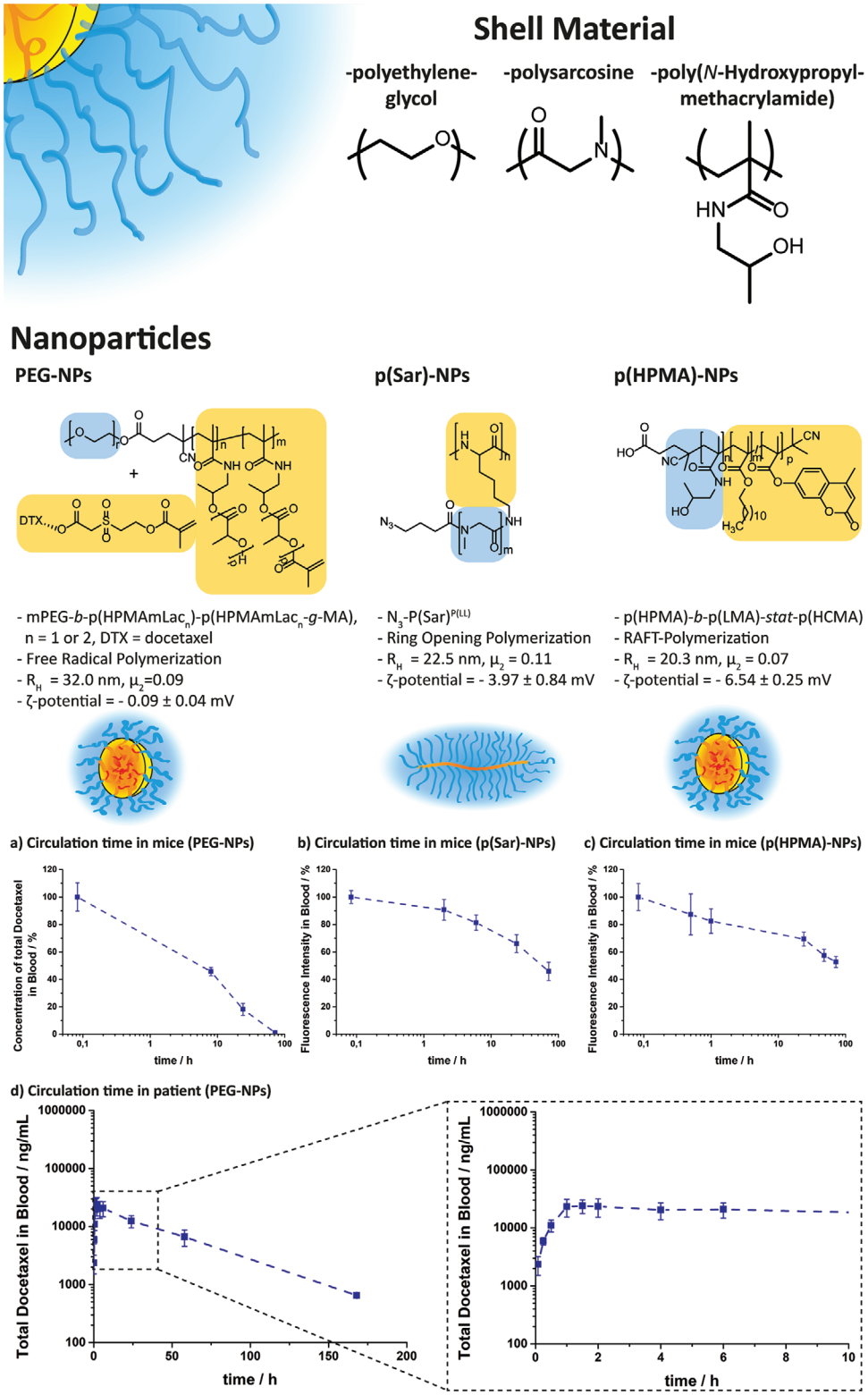

Figure 1. Overview of the hydrophilic shell materials of the characterized nanoparticles. Chemical structure of the utilized polymers, polymerization type, hydrodynamic diameter, polydispersity (μ_2) and zeta potential are shown. Circulation times of the three tested nanoparticles. a) Blood circulation time of the PEG-NPs in mice ($n = 3$). b) Blood circulation time of pSar-NPs in mice ($n = 5$). c) Blood circulation time of p(HPMA)-NPs in mice ($n = 5$). d) Blood circulation time of PEG-NPs in patient with progressive solid tumors ($n = 5$). Note, that the first measurement point for PEG NPs in mice and patient was 5 min post i.v. injection, for the p(Sar) NPs 5 min post i.v. injection, for p(HPMA) NPs 15 min post i.v. injection. 100% of docetaxel concentration and fluorescence intensity correspond to the concentration/intensity at the earliest time point.

© 2020 The Authors. Published by WILEY-VCH Verlag GmbH & Co. KGaA, Weinheim

For pSar (n = 5) and pHPMA NPs (n = 5) the pharmacokinetic profile was determined in Balb/c white mice (in case of pHPMA-NPs Balb/c mice bearing 4T1 tumors). For this purpose, both nanoparticles were labelled with a near-infrared dye via copper-free click chemistry (see experimental part). The experiments ex vivo (blood samples from in vivo experiments) revealed a prolonged blood circulation profile of both pSar and pHPMA NPs with blood half-lives above 24 h (see Figure 1b,c).

In the case of the PEG NPs, the blood half-life was determined by measuring total docetaxel (i.e., sum of already released and still bound) in the blood of mice (n = 3) and men (n = 5) with progressive solid tumors.[21,51] It is thus not one-to-one comparable to the labeled pSar and pHPMA NPs. Thereby it was found that—in mice—a single intravenous injection enabled complete regression of both small and established tumors. The systemic circulation of PEG NPs (CPC634) was obtained in a dose escalation phase 1 study.[52] The experiments revealed a blood half-life of 7.4 h in mice, but interestingly 31.6 h in men (see Figure 1a,d). These results indicate that the three nanoparticles investigated in this study circulate very well in vivo in mice. Prolonged circulation times are of major importance, since they enhance the chance for passive or active targeting and thus for accumulation in the tumor tissue. This could be verified for similar or identical structures of the tested nanoparticles (see section "Tumor accumulation of studied nanoparticles" in the Supporting Information). In addition and more important, the PEG NPs (CPC634) show excellent pharmacokinetics in patients.[52] Hereafter, we considered a comparative study of the interaction of the three nanoparticles with plasma proteins important to gain a better understanding of the role of protein affinity and protein corona formation on the circulation times.

To determine interactions with plasma proteins, the three nanoparticles were incubated in EDTA-stabilized, full human plasma (pooled from six healthy donors) for 1 h at 37 °C and continuously agitated (500 rpm) to simulate the conditions in the body, where diffusion of cells and proteins constantly occur in the blood flow. As previously shown, one hour of incubation is sufficient for protein corona formation.[53,54]

Since the separation of nanoparticles and plasma components by centrifugation is hardly possible for systems with densities comparable to plasma, such as polymeric micelles, we have chosen to apply asymmetrical flow field-flow fractionation for the separation of nanoparticles and plasma components. Here, we specifically optimized AF4 separation conditions for each nanoparticle allowing the exclusive elution of the incubated nanoparticles and their separation from the plasma proteins. The isolated nanoparticle–protein-complex was then measured by dynamic light scattering to characterize any size increase due to protein adsorption. Moreover, protein affinity was investigated qualitatively and quantitatively by sodium dodecyl sulfate polyacrylamide gel electrophoresis (SDS-PAGE) and label-free liquid chromatography-high-resolution mass spectrometry (LC-MS). A schematic illustration of the separation procedure is displayed in **Figure 2**.

Since most single proteins in blood plasma are in the size range of 6–10 nm,[55] thus smaller than the investigated nanoparticles, they are eluting prior to the nanoparticles in the AF4 channel (Figure 2).[19,26]

The AF4 elugrams for the three polymeric nanoparticles are shown in **Figure 3**a–c. A run of pure plasma is pictured in red resulting in an intense peak between 6.5 and 10 min at the beginning of the measurements, which consists of the main fraction of small proteins (larger objects like lipoproteins and particles aggregates appear—at the end of each measurement—in the rinse peak). The elugrams of nanoparticles, which were incubated with phosphate buffered saline (PBS) instead of plasma, are presented in green. Since the nanoparticles are larger than most of the proteins they are eluting later and depending on the crossflow at different retention times (see experimental part). The elugrams of the mixtures between nanoparticles and pure plasma after incubation are shown in blue. During the measurements we observed—for all three cases—no sign of any significant loss of particles or proteins by unspecific adsorption in the device (loss of UV-intensity or adsorption onto the membrane, see Figure S6 in the Supporting Information experiments to plasma loss) or aggregation in the AF4 channel. Furthermore, the nanoparticle peaks did not undergo any shift to later retention times after incubation (UV and MALS detector, for MALS detector see Figure S7 in the Supporting Information), which is a first indication that the size of the particles is not significantly altered during incubation with plasma. Nanoparticles, which aggregate with proteins and thus increase in size, would elute at later retention times or even during the rinsing due to the smaller diffusion coefficient of the aggregate (see examples for PS NPs and different micelles in Figure S8 in the Supporting Information). This fact was confirmed by multiangle-light scattering of isolated particles, which were incubated with plasma or PBS before purification by AF4 (Figure 3d–f). For all three nanoparticles the hydrodynamic radius remains the same, whether they were incubated in PBS or plasma. These results confirm our starting hypothesis that the chosen materials remain intact and are not subjected to any dynamics after exposure to plasma. Moreover, these results further indicate that there is no major adsorption of proteins on the nanoparticles leading to a significant size increase of the complexes, which is in accordance to findings on liposomes as determined by AF4.[19] On the other hand, a previous study with solid nanoparticles demonstrated corona formation induced changes in particle size as detected by dynamic light scattering (DLS) or retention time shifts in AF4.[26] This is in agreement with a recent study from Couffin and coworkers, which proved that with AF4 it is possible to detect small size differences (5–10 nm) between different nanoparticles.[56]

Since we did not observe any change of the hydrodynamic radii of the nanoparticles from possible adsorbed proteins, we conducted further experiments to identify potential corona proteins by SDS PAGE. **Figure 4**a shows a silver stained gel of the isolated fractions of the three nanoparticles, which were incubated in plasma and purified by AF4. For all three systems a distinct band between 50 and 60 kDa (Figure 4a, slot 4–6) is visible. As the same band is the most intensive one in 1% plasma in slot 1 of the gel, the detected protein could be identified as human serum albumin (HSA). Since HSA is the most abundant protein in human blood plasma,[57] traces of it are probably bleeding into other fractions. With this conclusion it is necessary to compare the matching fraction of a control

© 2020 The Authors. Published by WILEY-VCH Verlag GmbH & Co. KGaA, Weinheim

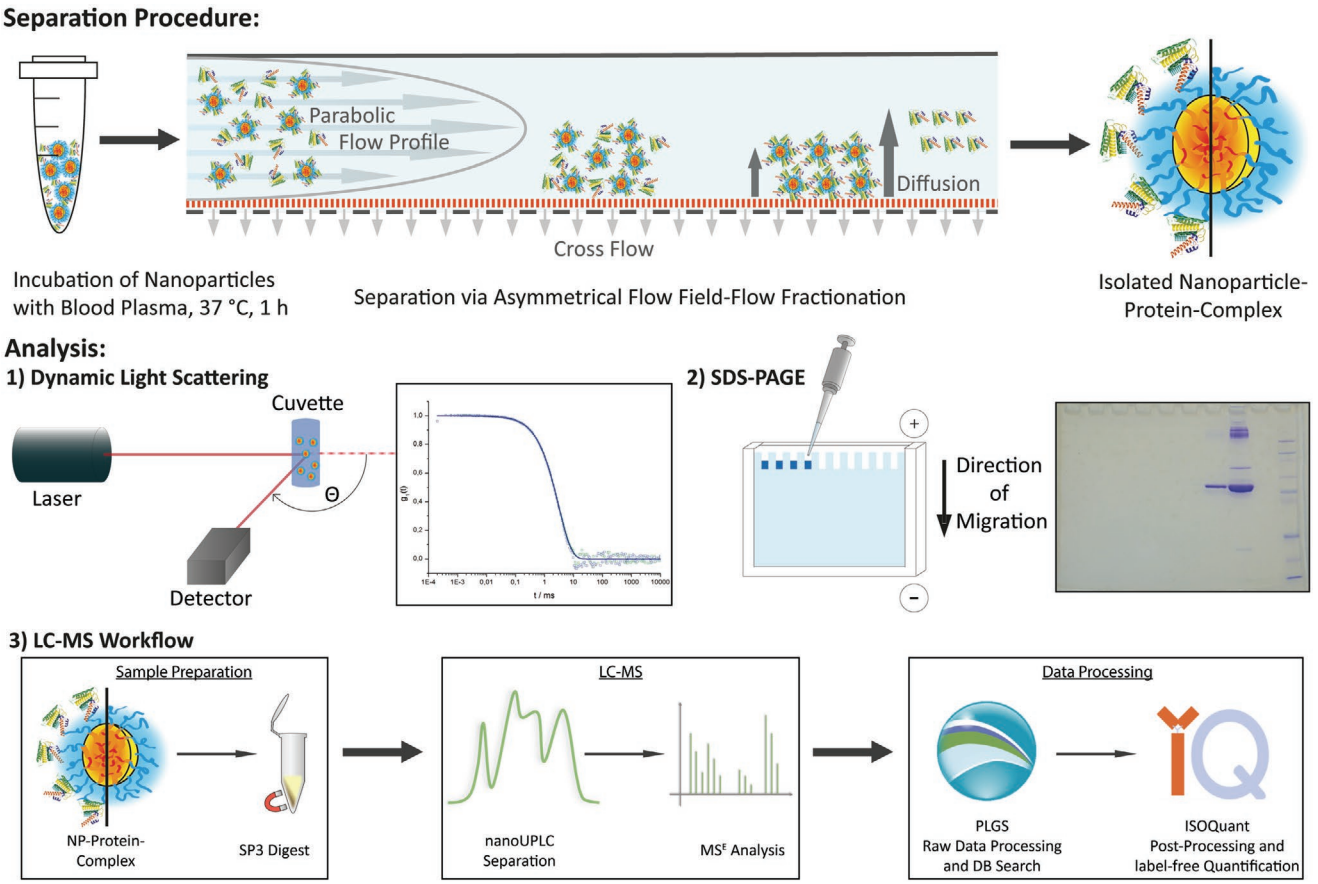

Figure 2. Separation procedure of nanoparticles and proteins via AF4 and analysis of the isolated nanoparticle–protein-complex. In a first step, the nanoparticles were incubated in full human blood plasma for 1 h at 37 °C. After the incubation, the particles were separated via asymmetrical flow field-flow fractionation (AF4) from unbound proteins and isolated for further analysis. The size of the NP-protein-complex was characterized with multi-angle light scattering for detection of possible size increase due to protein adsorption. SDS PAGE and label-free quantitative proteomic analysis revealed the composition and amount of enriched proteins on the nanoparticles.

AF4 run with pure plasma (without nanoparticles). Figure 4a shows this fraction for the three nanoparticles in slot 8–10, respectively. Both in the fraction of the control plasma run and the run using nanoparticles incubated with plasma there is an albumin band visible, indicating that HSA, as the most abundant protein, is in fact co-eluting with the nanoparticles. Nevertheless, the amount of albumin is still very low, since it could only be detected with the very sensitive silver staining, which has a detection limit in the sub-nanogram range.[58] (Coomassie stained gels did not reveal any bands on both fractions for each system (Figure S9, Supporting Information)).

To quantify the total amount of HSA (coeluting or adsorbed) in the purified nanoparticle fraction, we performed two sets of experiments. First, we compared the nanoparticle fraction with molecular polymer brushes, which had been chemically functionalized with an average of 2 or 10 antibodies, by SDS-PAGE (see Figure S10 in the Supporting Information). These experiments indicate that the total amount of coeluting or adsorbed proteins on the purified brushes (after AF4) is smaller than 2 antibodies per brush. To further characterize the proteins in the nanoparticle fraction, we performed a comparative SDS-PAGE-based analysis of AF4 separated fractions with various amounts of free, pure HSA (Figure 4b). The amount of HSA in the fraction of the purified brushes was determined to be 5–10 ng per 730 ng of brushes, i.e., on average less than one molecule HSA per brush. For the other types of nanoparticles, a comparably low amount of HSA was only detected (calculations in the Supporting Information). Thus, even if all HSA would be stably attached to the different nanoparticles, this can hardly be regarded as a bona fide protein corona, as less than 1 molecule of albumin per particle would lead to a neglectable surface coverage of the nanoparticles.

Our SDS-PAGE analyses indicated that besides albumin there are also various other proteins detectable in the fraction of the purified nanoparticles in trace amounts (less than albumin). Notably, most of them could also be found in the control plasma run, which indicates that these proteins are—at least to some extent—coeluting during AF4 (see Figure 4a).

We hypothesized that "true corona components" should be significantly enriched in AF4 runs of plasma-incubated nanoparticles relative to control fractions from pure plasma and pure particle runs. Therefore, to identify potential corona proteins, we performed a label-free quantitative proteomic analysis to quantify the relative protein amounts within the AF4 fractions, comparing the incubated particle containing fractions and the respective control fractions from plasma runs (without

© 2020 The Authors. Published by WILEY-VCH Verlag GmbH & Co. KGaA, Weinheim

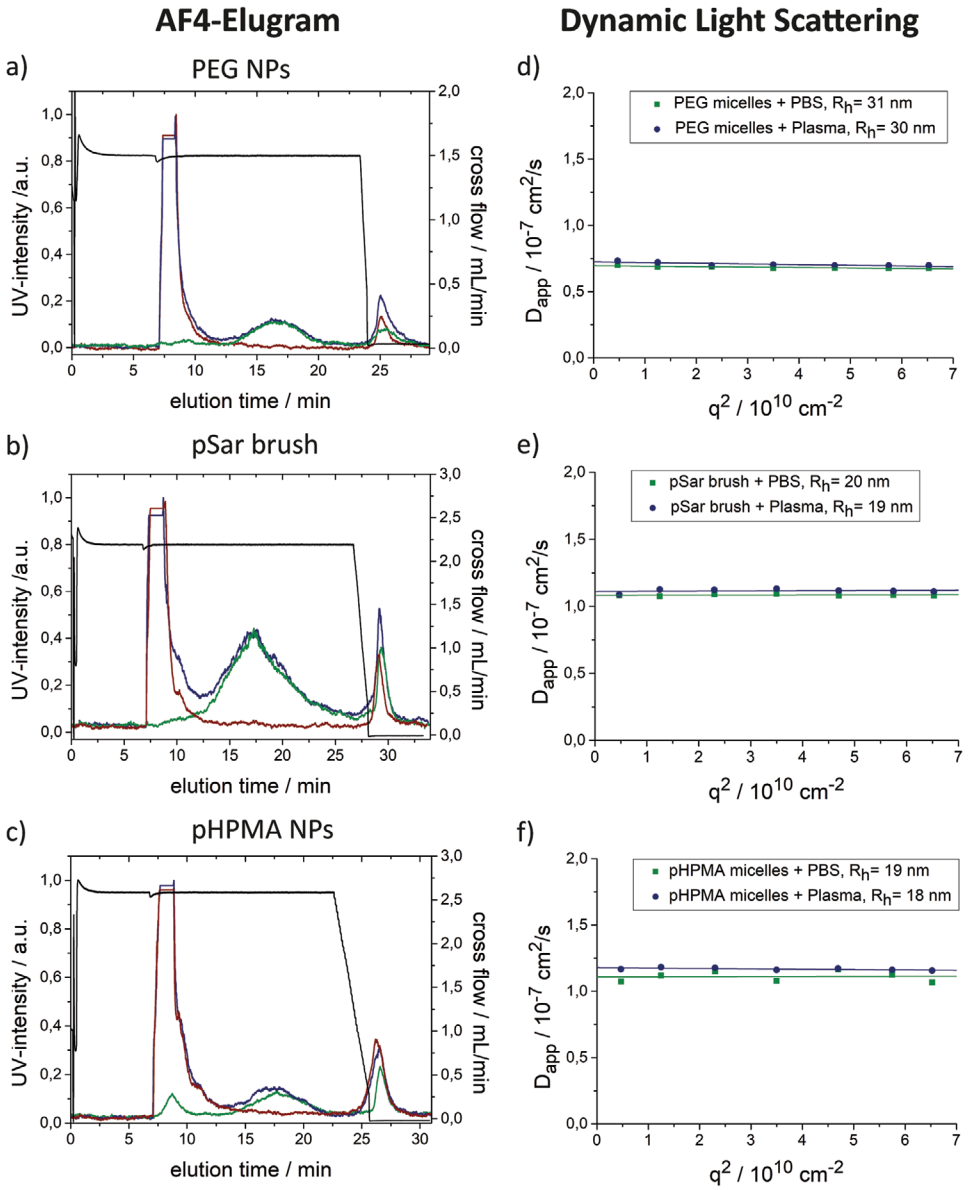

Figure 3. a–c) AF4 elugrams of characterized NPs (green), plasma (red), and in plasma incubated NPs (blue): a) for PEG-NPs; b) for p(Sar) NPs; c) for p(HPMA)-NPs. d–f) Apparent diffusion coefficient versus scattering vector of in PBS (green) and in plasma (blue) incubated NPs after isolation with AF4: d) for PEG-NPs; e) for p(Sar)-NPs; f) for p(HPMA)-NPs. AF4 elugrams for all three nanoparticles are showing that there is no major size increase or aggregation formation due to nanoparticle–protein-interactions. For all three NPs the hydrodynamic radii did not increase due to possible protein adsorption. Also, the diffusion coefficient is identical at seven different scattering angles (30°, 50°, 70°, 90°, 110°, 130°, 150°) indicating a narrow size distribution of all three nanoparticles.

NPs). For this purpose, we applied our recently described SP3-based protocol to obtain maximal sensitivity of the quantitative proteomic analysis.[59]

In the AF4 fractions obtained after particle incubations with plasma, we quantified 126 proteins for p(Sar)-NPs, 146 for p(HPMA)-NPS, and 128 proteins for PEG-NPs (excluding trypsin and human keratins). Our analyses confirmed that HSA constituted the major component of the proteins detected in the AF4 fractions of all particles (29.6–40.6% of detected potential corona components) (Figure S11, Supporting Information). However, it was not significantly enriched compared to the respective elution ranges (plasma without particles) in AF4.

This strongly indicated that a simple detection approach (as often used in corona analysis) may result in false positive assignments of corona proteins, as our analyses indicate most proteins detected by the proteomic analysis of the AF4 fractions are in fact plasma proteins that simply co-elute with the NPs during AF4 or are previously bound to the particle. Without the analyses of the respective negative controls, and subsequent comparative analysis between plasma incubation fractions and the respective elution range of plasma without particles or of particles without plasma, these proteins would likely have been erroneously assigned as constituents of the protein corona.

© 2020 The Authors. Published by WILEY-VCH Verlag GmbH & Co. KGaA, Weinheim

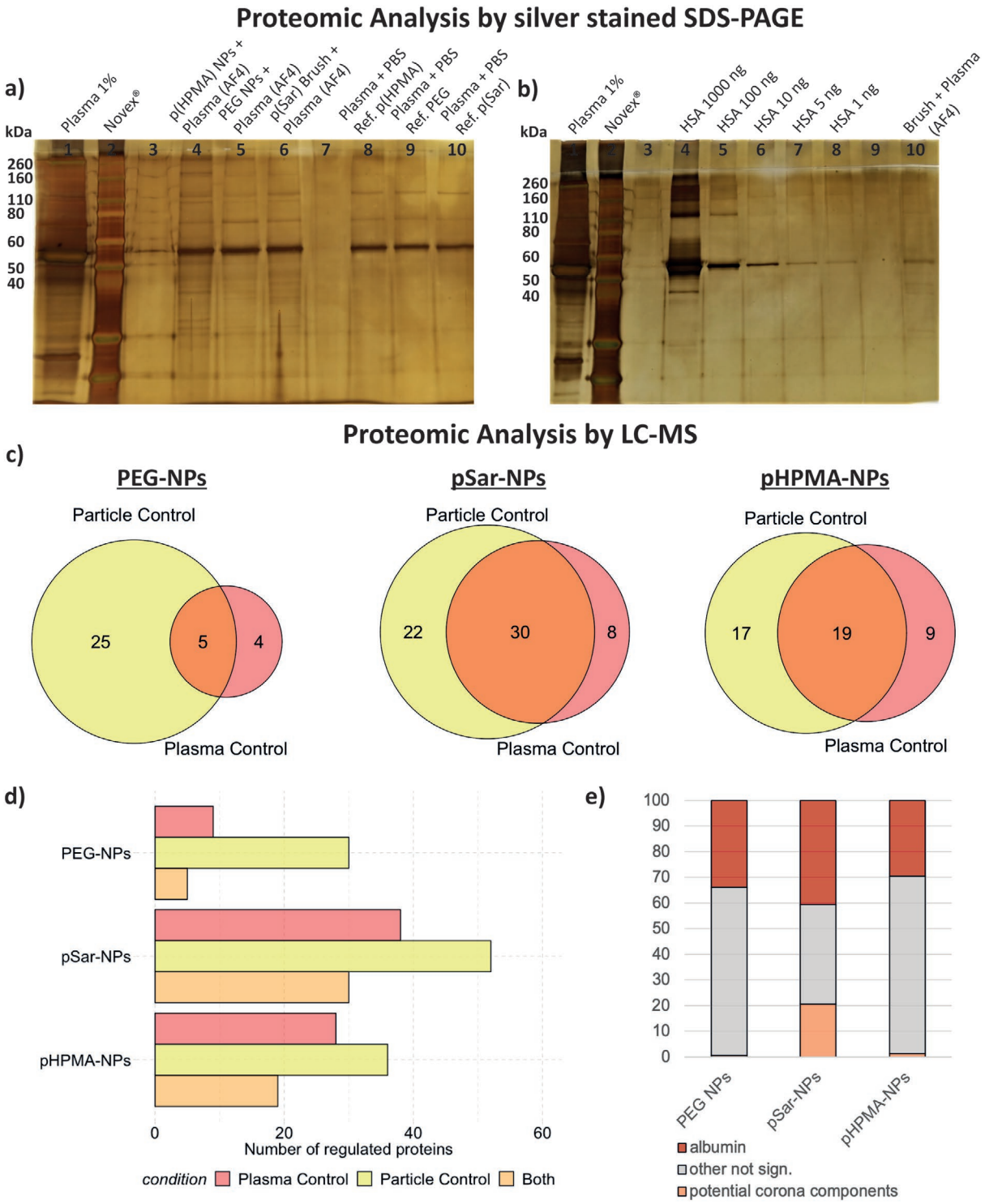

Figure 4. a) Silver stained gel of isolated fractions of p(HPMA)-, PEG-, and p(Sar)-brushes after AF4 purification. 1) Human blood plasma 1%, 2) Novex Sharp Pre-Stained Protein Standard, 3) Empty, 4) p(HPMA)-NP + plasma, 5) PEG-NP + plasma, 6) p(Sar)-brush + plasma, 7) Empty, 8) Plasma and PBS in elution area of p(HPMA)-NP, 9) Plasma and PBS in elution area of PEG-NP, 10) Plasma and PBS in elution area of p(Sar)-brush; b) Silver stained gel of isolated p(Sar)-brushes after AF4 purification and Human Serum Albumin at different concentrations. 1) Human blood plasma 1%, 2) Novex Sharp Pre-Stained Protein Standard, 3) Empty, 4) HSA 1000 ng, 5) HSA 100 ng, 6) HSA 10 ng, 7) HSA 5 ng, 8) HSA 1 ng, 9) Empty, 10) Brush and plasma after AF4; c) Venn-Diagrams for enriched proteins on NPs. The overlap area shows the number of proteins significantly enriched in the sample compared to both control conditions. d) number of enriched proteins for all particles and conditions. e) Each bar represents the complete amount of protein detected in the sample shown as average across all biological and technical replicates. Red reflects the percentage share of HSA, grey all other proteins and orange shows the partition of the significantly enriched proteins (i.e., the protein corona).

© 2020 The Authors. Published by WILEY-VCH Verlag GmbH & Co. KGaA, Weinheim

In our experimental setting, a protein that shows enrichment only in the particle control condition (plasma incubated particles compared to pure particle run) is most likely co-eluting, since all contaminants (proteins bound to the particle before) are not upregulated.

A protein that shows upregulation only in the plasma control condition (plasma incubated particles compared to pure plasma run) is regarded as a potential contaminant, because in this condition co-eluting proteins are not upregulated.

Consequently, we consider only those proteins that are significantly enriched in both conditions at a time as parts of a potential protein corona (see also section "Explanation Protein Corona Analysis" in the Supporting Information). These conditions are met for only five proteins for the PEG-NPs. 19 proteins were enriched in both conditions on p(HPMA)-NPs and 30 proteins on p(Sar)-NPs (Figure 4c,d; Table S1, Supporting Information).

Of the 30 protein entries identified as enriched in both conditions on p(Sar)-NPs, 17 are variants of Immunoglobulins subdomains (representing less than 17 full proteins) and 5 of them are keratins (likely derived from sample handling, therefore not relevant) which means that only 8 proteins (APOD, CXCL7, LG3BP, CD5L, S10A8, HRG, ANXA2 and CO3) that do not belong to these protein classes are potentially enriched on the particle. The same holds true for p(HPMA)-NPs, where 5 immunoglobulin entries and two keratins were significantly enriched, resulting in only 12 proteins (HPTR, KI21B, SAMP, ENOA, TGM3, IC1, ITIH4, HSPB1, SAA4, APOH, CLUS and KPRP) potentially bound to the particle surface. In addition to three Immunoglobulin entries, only two proteins (ANXA2 and HORN) were identified as enriched on PEG-NPs. Enriched proteins are listed in Tables S2–S4 in the Supporting Information.

As this seemed to indicate a protein corona formation for all particle systems, we next investigated the absolute amounts of proteins significantly enriched on the respective particles relative to the total amount detected in the AF4 fractions. Here, we determined the average ppm value for each protein across all technical and biological replicates (except of contaminants) and calculated their contribution to the total protein abundance.

While albumin (not significantly enriched) constituted 30–40% of total protein, the relative percentage of the significantly enriched proteins on the particles contributed little to the total amount of protein identified in the AF4 fractions for the three systems investigated. Our analyses revealed that the significantly enriched proteins represent 20.58%, 1.32%, and 0.53% of the total amount of protein on the p(Sar)-, p(HPMA)-, and PEG-NPs, respectively (Figure 4e). Since we calculated the amount of HSA to be less than one molecule per particle, the amounts of significantly enriched proteins therefore have to be much less, also for the pSar-NPs, for which the amount of enriched proteins is with 20.58% (of less than one) the highest. An amount of 20% of maximum one protein per nanoparticle would be 2 proteins for 10 nanoparticles. These findings mean that on average 80% of the nanoparticles are not associated with a single protein. Consequently, our analyses show that the large majority of nanocarrier systems used in this study do simply not possess a protein corona. This result opens the question why only a few percent of the NPs interact with proteins and whether this is an intrinsic property of the nanoparticles or more a result of some special arrangement of constituents in some nanoparticles (e.g., unreacted crosslinkable groups or remaining primary amines (positively charged under physiological conditions)) that are the basis for the detected, selectively enriched proteins. We need to state clearly that further research is required to fully understand the underlying principles on a molecular level.

Taken together our results from proteomic analysis indicate that all three NPs show a neglectable formation of a stable protein corona, which is in perfect agreement with the performed DLS and SDS-PAGE measurements. This low amount of enriched proteins validates the absence of—what is usually termed as—a hard protein corona on these NPs. For pSar-NPs this is also in line with the FCS study in full blood by Negwer et al.[42]

Concerning the boundary conditions: these results apply after an in vitro incubation of one hour and during a separation protocol, which allows the diffusion of proteins away from the nanoparticle during their flow in PBS buffer. Thus, the AF4 experiment cannot exclude a very weak protein affinity (very soft corona with reversible binding), whereby (primarily) enriched proteins could diffuse away during separation by AF4. In this context it is, however, important to mention that there are good indications that AF4 is capable to isolate the nanoparticles including the soft corona.[26] Also, an in vivo incubation of these nanoparticles in the body could possibly lead to a larger amount of enriched proteins as reported by Dawson, Kostarelos and coworkers for liposomal nanoparticles recollected from the blood of animals[25] and patients.[60]

The difference in corona formation compared to colloidal nanocarriers is probably a consequence of the chemical structure of the core crosslinked micellar architectures studied here (see Figures S1 and S2 in the Supporting Information). All studied polymeric nanocarriers provide a dense hydrophilic corona (for a rough estimation of the grafting density see the Supporting Information), which is covalently stabilized by core-crosslinking. Therefore, the studied nanoparticles are of a stable nature in plasma and do not face rearrangements of their internal structure (see ref. [17] and section "Comparison between nanoparticles with a hard interface and polymeric micellar structures" in the Supporting Information for discussion). Thus, it is, e.g., not possible that shielding domains may rearrange spontaneously and expose hydrophobic patches, where plasma proteins can adsorb and build up a protein corona irreversibly.

Thus, obviously, nanoparticles are not all alike and interact differently with plasma proteins, whereby the variability extends from only some nanoparticles interacting with a protein to the formation of an extensive protein corona on each particle. This also is in agreement with results obtained previously for other systems like nanoparticles coated with zwitterionic structures[61,62] and self-assembled systems such as some liposomes, where the detected amount of proteins was also small and much lower than for polystyrene and silica colloids.[19] In the case of a zwitterionic coating the strong electrostatic binding of water is claimed to be responsible for the small protein affinity. Concerning the mentioned liposomes, it seems intuitive that such materials, which are relatively similar to natural structures, would in general also reduce interaction with proteins. And—in fact—the reduced amount of proteins on these liposomes led to a situation, where the subsequent biological response was only determined by the functional groups on the

© 2020 The Authors. Published by WILEY-VCH Verlag GmbH & Co. KGaA, Weinheim

surface.[19] This is beneficial for active targeting and might be beneficial for clinical applications, as potential negative effects of the protein corona are unlikely to impede the pharmacokinetic parameters of these NPs.

In addition, our data underline the importance of appropriate negative controls and background subtraction when applying AF4 (or other size-exclusion-techniques) in combination with the highly sensitive mass spectrometric workflows for protein corona analysis to avoid misleading conclusions.

3. Conclusion

Our results demonstrate that only a neglectable amount of plasma proteins is found on polymeric nanocarriers with dense surface coatings of PEG, pSar or pHPMA. None of the nanoparticles increased in size after incubation and isolation from human plasma, while only non-significant signs of proteins could be detected applying SDS-PAGE with the very sensitive silver staining (subnanogram detection). Interestingly, the amount of plasma proteins is found to be significantly less than one equivalent human serum albumin protein (66 kDa) per nanocarrier for all the three evaluated systems. Thus, most of the nanocarriers are not associated with any protein at all. This is clearly much less protein adsorption than previously observed for other colloidal nanoparticles[10,26,63] and it does by no means correspond to a dense protein corona as it is often discussed for nanoparticles. Therefore, intensive corona formation is not a general property of nanoparticles, which is in accordance with recent findings for nanoparticles coated with zwitterionic structures[61,62] and some liposomes.[19]

It is, however, noteworthy that even under these conditions it is possible to identify the enriched proteins in the fractions of the studied polymeric nanocarriers by applying label-free quantitative proteomic analysis with mass spectrometry. Nevertheless, the presented methodology requires negative controls and carefully conducted background subtraction techniques to avoid misleading conclusions.

Since all nanocarriers provide significantly high plasma circulation times, our results clearly demonstrate that this is a property of the carrier system itself and cannot be explained by protein corona formation. These findings may explain the neglectable patient variability of PEGylated polymeric nanocarriers in clinical phase II (CPC634),[21,52] and underline the potential of PEG, pSar and pHPMA-based carriers in nanomedicine.

4. Experimental Section

Materials: A 20-fold stock solution of the used phosphate buffered saline was prepared out of sodium chloride, potassium chloride, disodium phosphate and potassium phosphate with a final salt concentration of 151.7 mmol L^{-1}. The stock solution was also filtrated (Millipore GHP 0.2 µm) before using it in the AF4 system.

Human blood plasma was provided from the Transfusionszentrale of the Medical Department of the Johannes Gutenberg-University Mainz. It was pooled of six healthy donors and stabilized with EDTA.

Synthesis of pHPMA-NP: Analogous to the protocol of Kramer et al.,[48] core-crosslinked p(HPMA) micelles were prepared out of amphiphilic poly(*N*-(2-hydroxypropyl) methacrylamide)-*b*-poly(lauryl methacrylate-*ran*-hymecromone methacrylate) block copolymers by solvent switching. After obtaining the micelles the hymecromone units in the hydrophobic block were dimerized in a [2 + 2] photocycloaddition by UV light irradiation to provide a core-crosslinking of the micelles. The p(HPMA)-*b*-p(LMA-*ran*-HCMA) polymer was synthesized via RAFT polymerization of PFPMA with 4-cyano-4-((thiobenzoyl) sulfanyl)pentaonic acid as CTA and AIBN as initiator. In a second step the p(PFPMA) homoblock was deployed as a macro-CTA for the polymerization of LMA and HCMA. After removing the dithiobenzoate end group the p(PFPMA)-*b*-p(LMA-*ran*-HCMA) precursorpolymer was transferred with 2-hydroxyaminopropanol via aminolysis into p(HPMA)-*b*-p(LMA-*ran*-HCMA).

Synthesis of PEG-NP: Core crosslinked nanoparticles containing covalently entrapped docetaxel (CPC634) were prepared and characterized as fully described in detail before.[21]

Synthesis of pSar-Brushes (pSar-NP): PSar brushes were prepared and characterized as fully described in detail before.[49] In addition, after the full Sar-NCA conversion, the secondary amine end groups of the pSar brushes were quenched with azido butyric acid pentafluorophenyl ester introducing terminal azide functionalities for subsequent selective conjugation of biologically active substrates.

Synthesis of Cyanin7 Functionalized pHPMA NPs: Poly(*N*-(2-hydroxypropyl) methacrylamide)-*b*-poly(lauryl methacrylate-*ran*-hymecromone methacrylate) block copolymers for cyanin7 functionalized pHPMA micelles were synthesized analogous to the unfunctionalized pHPMA NPs but by using an azide-functionalized CTA for RAFT polymerization.[64,65] After preparation and crosslinking of the micelles they were functionalized with cyanin7-DBCO from Lumiprobe. For the functionalization step a DMSO-water-solution (65:35, v:v) of Cyanin7-DBCO was added to a PBS solution of the crosslinked micelles in a molar ratio of 1 to 3 (dye to polymer) and the reaction solution was stirred (500 rpm) overnight at 35 °C. The reaction solution was then filtrated with Amikon Ultra Centrifugal Filters from Merck Millipore with a regenerated cellulose membrane and a molecular weight cut off of 30 kDa and washed with 20 mL Milli-Q water to remove free dye. Subsequently the solution was further purified via HPLC. Preparative size exclusion chromatography was performed via an Agilent 1100 System (Agilent, Germany). A volume of 100 µL of the NP solution was injected into the system running with PBS at a flow rate of 1 mL per min. A BioRad UNO Q1 column (BioRad, Munich, Germany) filled with Sephajzz S-500 (GE Healthcare) was used for separation. A multiwavelength detector (G1365A Agilent 1100 Series, Germany) was used for the detection of the absorption of Cyanin7-labeled NPs. An automated fraction collector collected the resulting purified NP solution.

Synthesis of Functionalized pSar-Brushes (Dye 800 CW and Antibody aDEC205)—Dye labeling: The dye 800CW-DBCO was conjugated to the pSar brushes via SPAAC. In a typical experiment, brushes were dissolved in PBS ($\beta = 50$ g L^{-1}) and the dye was dissolved in DMSO ($c = 5 \times 10^{-3}$ M). As the reaction was quantitative, 1 equivalent of the desired amount of dyes per brush was added. After incubation (continuous agitation at 550 rpm) overnight at 20 °C under light exclusion, the reaction mixture was purified by Amicon Ultra Centrifugal Filter Devices to remove unbound dye and DMSO (15 mL, 50 kDa, 4000 × *g*, 10 times). The resulting solution was concentrated with Amicon Ultra Centrifugal Filter Devices (50 kDa, 4000 × *g*), filtered through sterile 0.22 µm Millex-GS filters and stored at –20 °C.

Synthesis of Functionalized pSar-Brushes (Dye 800 CW and Antibody aDEC205)—Synthesis of DBCO-Functionalized aDEC205 Antibodies: In a typical experiment, 2 eq. DBCO-PEG4-NHS-Ester (dissolved in DMSO, c = 10 g L^{-1}) were added to aDEC205. aDEC205 was used as received (dissolved in buffer, c(aDEC205) = 4,7 g L^{-1}). After incubation (continuous agitation at 550 rpm) overnight at 20 °C, the reaction mixture was purified by Amicon Ultra Centrifugal Filter Devices (15 mL, 10 kDa, 4000 × *g*, 10 times) to remove unbound DBCO-PEG4-NHS-Ester, NHS and DMSO. Afterward preparative SEC was performed using a Sepharose 4 FF XK 16/70 column (flow 0.5 mL min^{-1}) to remove aggregates. The resulting solution was concentrated with Amicon Ultra Centrifugal Filter Devices (10 kDa, 4000 × *g*), filtered through sterile 0.22 µm Millex-GS filters and stored at –20 °C. Yield: 80–90 %.

© 2020 The Authors. Published by WILEY-VCH Verlag GmbH & Co. KGaA, Weinheim

Synthesis of Functionalized pSar-Brushes (Dye 800 CW and Antibody aDEC205)—Synthesis of aDEC205 pSar Brushes: The amount of the DBCO-modified aDEC205 antibody that needs to be added depends on the number of DBCO per antibody (*N*_DBCO between 1–2). 1/(0.34·*N*_DBCO) equivalents of the DBCO antibody (dissolved in PBS, c(aDEC205-DBCO) = 5–15 g L^{-1}) were added to the pSar brush dissolved in PBS (c = $1 \cdot 10^{-5}$–$1 \cdot 10^{-6}$ M). The reaction mixture was incubated (continuous agitation at 550 rpm) overnight at 20 °C. To remove bridged brushes and unconjugated bioactive components, brush-conjugates were purified via preparative SEC using a Sepharose 4 FF XK 16/70 column (flow 0.5 mL min^{-1}). The fractions were concentrated using Amicon Ultra Centrifugal Filter Devices (50 kDa, 4000 × *g*), filtered through sterile 0.22 µm Millex-GS filters and stored at –20 °C.

In Vivo Experiments—Circulation Time of pSar Brushes in Mice: For determination of the circulation time BALB/c mice were anesthetized with isoflurane prior to injection of the 800CW functionalized pSar brushes (150 µL in PBS (c(Dye) = 1.5×10^{-5} M) intravenously and blood kinetics were determined by retrieval of blood at indicated time points. Briefly, retrieved blood samples (50 µL) were collected in a black 96-well plate and fluorescence intensities were determined with the IVIS Spectrum Imaging system (Perkin Elmer) using the filter set at 745 nm for excitation and at 800 nm for emission with an integration time of 3 s.

In Vivo Experiments—Circulation Time of pHPMA NPs in Mice—Animal Preparation: All mice were inhalation-anesthetized with 4.0% isoflurane in oxygen-enriched air in a mouse induction chamber and with 2.0% isoflurane in oxygen-enriched air with a face mask during all experimental procedures. All animal experiments were approved by local and institutional ethical committees. 6–8 weeks old BALB/cAnNRj female mice (Janvier Labs, France) were used to have a syngeneic mouse model due to the fact that the 4T1 breast cancer cells were collected from identical individuals. Thus, the syngeneic BALB/c mouse model allows to study how cancer therapies perform in conjunction with a functional immune system and serve as a surrogate for human patients. The mice were kept in pathogen-free cages having their own ventilation and placed in rooms with controlled 12 h light/dark cycles. Mouse 4T1 breast cancer cells (American Type Culture Collection, Manassas, VA, USA) were cultured in RPMI medium (RPMI 1640; Gibco, Life Technologies GmbH, Germany), supplemented with 10% fetal bovine serum (FBS; Life Technologies GmbH, Germany) and 1% penicillin/streptomycin (10000 U mL^{-1} penicillin; 10 mg mL^{-1} streptomycin, Life Technologies GmbH, Germany), at 37 °C and 5% CO_2 in a humid atmosphere. Tumors were induced by inoculating 2.5 × 104 4T1 cells orthotopically into the right abdominal mammary gland of the mice. Tumors were allowed to grow for 10 days, until they reached a size of 5 mm in diameter. The weight and tumor size were controlled every day.

In Vivo Experiments—Circulation Time of pHPMA NPs in Mice—CT-FLT Imaging: For intravenous probe injection, a sterile catheter was placed into the lateral tail vein of the mouse. The catheter was prepared beforehand by connecting a 30 G cannula (B.Braun, Melsungen, Germany) to a polyethylene tube with an inner diameter of 0.28 mm and outer diameter of 0.61 mm, and a wall thickness of 0.165 mm (Hartenstein, Würzburg, Germany). At a tumor size of 5 mm all mice were i.v. injected with the cyanin7-labeled pHPMA nanoparticles (2 nmol; in 50 µL 0,9% NaCl sterile solution) for quantifying the biodistribution and blood circulation time (data on biodistribution is shown in Figure S15). The blood was taken from the tail vein at different time points to measure the blood half-life over 72 h. After the last CT-FLT scan, the animals were sacrificed, and organs were excised for ex vivo evaluation.

In Vivo Experiments—Circulation Time of PEG NPs in Mice: For determination of the circulation time BALB/c mice were anesthetized with isoflurane prior to intravenous injection of the PEG NPs (CPC634).[21] The dose of CPC634 was determined by the body weight of each mouse (30 mg kg^{-1}). Blood kinetics were determined by retrieval of blood at indicated time points. Retrieved blood samples were collected and the concentration of total docetaxel (still covalently entrapped plus already released) was determined via LC-MS/MS as described in.[51]

In Vivo Experiments—Circulation Time of PEG NPs in Patients: The circulation time of PEG-NPs (CPC634) was obtained in the context of a dose escalation phase 1 study of CPC634. Patients with solid tumors with no treatment options were included. The dose of CPC634 was determined by the body surface area of each patient (60 mg m^{-2}). CPC634 was administered i.v. as an 1 h infusion. Blood samples were taken at indicated time points and the concentration of total docetaxel (still covalently entrapped plus already released) was determined via LC-MS/MSas described in.[51]

Incubation with Human Blood Plasma: All nanoparticles (30 mg mL^{-1}) were incubated with EDTA-stabilized, pure and undiluted plasma 1:1 (v:v) at 37 °C for 1 h. The concentration of nanoparticles during plasma incubation was thus higher than during possible in vivo scenario, for which they were calculated to be 0.133 mg mL^{-1} the in the blood pool.[66] For a sufficient separation, the AF4 was limited to a maximal plasma concentration of 5 vol%. Therefore, after incubation the samples had to be diluted with PBS to a particle concentration of 1.5 g L^{-1} and a 5 vol% solution of plasma and immediately measured in AF4.

Thus, to enable an incubation of the nanoparticles with undiluted plasma, the initial particle concentration had to be high, since the mixture had to be diluted before the AF4 measurement.

Separation by AF4: The AF4 measurements were performed using an installation from the ConSenxuS GmbH. The setup was composed of a constaMETRICR 3200 main pump and a Spectra Series UV150 detector from Thermos Separation, a Dark V3 LS Detector from ConSenxuS GmbH, a Pharmacia P-3500 injection pump, a LV-F flow controller from HORIBA ATEC, a Waters In-Line Degasser-AF, and a separation channel with a 190 µm spacer and a reg. cellulose membrane with a molecular weight cutoff of 10 kDa, which was suitable for protein separation.[67] For the measurements with the PS NPs the UV absorption was detected at a wavelength of 280 nm, the UV absorption of all other NPs was detected at 220 nm. For all measurements except of those with polystyrene particles phosphate buffered saline (151.7×10^{-3} M) was used as solvent. For the polystyrene particles on the contrary—used as reference, shown in Figure S8 in the Supporting Information—a sodium chloride solution (4×10^{-3} M) was chosen and polyoxyethylen(20)-sorbitan-monolaurate (0.04×10^{-3} M) was added as detergent. Both solvents contained also sodium azide in a concentration of 0.2×10^{-3} M. The main flow was 1 mL min^{-1} higher than the crossflow for each measurement. For each nanoparticle the crossflow is illustrated in the respective AF4 elugram. Every measurement was carried out at least three times from three independent incubation experiments. Nanoparticle fractions were collected from 13.3 to 16.6 min for PEG NPs, from 16.6 to 20 min for pSar NPs and from 15 to 18.3 min for pHPMA NPs. To increase the concentration of the collected fractions from the AF4 after the separation process, they were filtrated with Amikon Ultra Centrifugal Filters from Merck Millipore with a regenerated cellulose membrane and a molecular weight cut off of 3 kDa. Since even the smallest plasma proteins (such as β2 microglobulin) has a molecular weight of >10 kDa,[68] there should be no loss of proteins during the spin filtration.

Remark to the Rinse Peak: The rinsing was performed at the end of every measurement and was not part of the actual measurement. It consists of contributions from the general setup and it contains larger aggregates. So, it cannot be highly interpreted.

In these experiments, the rinse peak did not change during plasma incubation, so there was no sign of aggregation behavior (see also MALS detector in Figure S7 in the Supporting Information). On the other side, when aggregation between particles and proteins happens as shown in Figure S8 in the Supporting Information, it increases strongly.

But the particle and rinse peak of the characterized systems did not change (see also MALS detector in Figure S7 in the Supporting Information), so there was no sign of aggregation behavior and therefore no need to characterize the eluting fraction in the rinse time.

SDS PAGE: The SDS-PAGE experiments were performed following the general protocol of Laemmli.[69] The polyacrylamide gels were composed of a 12%-separation gel (with 8% stacking gel) and the electrophoresis was carried out for 45 min at 200 V with a Mini-PROTEAN Tetra Vertical electrophoresis-chamber from BIO-RAD. 7.5 µL of each sample was

© 2020 The Authors. Published by WILEY-VCH Verlag GmbH & Co. KGaA, Weinheim

incubated with 2.5 µL loading buffer (NuPAGE LDS Sample Buffer, Invitrogen) for 5 min at 95 °C. Novex Sharp Pre-Stained Protein Standard from INVITROGEN was loaded on each gel as a protein ladder for comparison. The proteins in the gels were visualized using a Coomassie Blue treatment and a silver staining.

DLS: For dynamic light scattering experiments the collected fractions from the AF4 were prepared in a dustfree flowbox. They were filtered with syringe filters from PALL Life Science with a diameter of 13 mm and a GHP membrane (0.2 µm pores) into dust free cylindrical scattering cells (Suprasil, 20 mm diameter). The measurements were performed with a Uniphase He/Ne Laser (632.8 nm, 22 mW), an ALV-SP125 Goniometer, an ALV/High QE APD-Avalanche photodiode, an ALV5000/E/PCI-correlator and a Lauda RC-6 thermostat unit. All angular dependent measurements were carried out in 20° steps between 30° and 150°. Data analysis was performed according to the procedure described by Rausch et al.[55,70]

Zetapotential: For zeta potential analysis, a Malvern Zetasizer NanoZS was used. Samples were prepared at 1 mg mL^{-1} in a sodium chloride (10×10^{-3} M) solution. Each sample was independently measured 5 times and analyzed by its mean average and standard deviation.

Protein Digestion: Lyophilized protein corona proteins were digested according to the SP3 ("Single-Pot Solid-Phase-Enhanced Sample Preparation") protocol.[59] After solubilization in SDS-Lysis buffer (1% SDS, 1× complete Protease Inhibitor Cocktail-EDTA, 50×10^{-3} M HEPES, pH 8,5), proteins were reduced by adding 5 µL of 200×10^{-3} M Dithiothreitol (DTT) per 100 µL lysate (45 °C, 30 min). Free cysteines were subsequently alkylated by adding 10 µL 100×10^{-3} M Iodoacetamide (IAA) per 100 µL lysate (Room temperature, 30 min, in the dark). Subsequently, remaining IAA was quenched by adding 10 µL 200×10^{-3} M DTT per 100 µL lysate. Magnetic carboxylate modified particles Beads (SpeedBeads, Sigma) were used for Protein Clean-up and Acetonitrile (ACN), in a final concentration of 70%, was added to the samples to induce the binding of the proteins to the beads by hydrophilic interactions (Room temperature, 18 min). By incubating the bead-protein mixture on a magnetic stand for 2 min, the sample was bound to the magnet and the supernatant was removed, followed by two washing-steps with 70% ethanol (EtOH), addition of 180 µL ACN, incubation for 15 s and removal of the solvent. Finally, 5 µL digest buffer (50×10^{-3} M ammonium bicarbonate, 1:25 w/w trypsin:protein ratio) were added to the air-dried bead-protein mixtures and incubated over night at 37 °C. To purify peptides after digestion, ACN was added to a final concentration of 95%. After another washing step (s. Sielaff et al., 2017 for detailed information) the beads were resuspended in 10 µL 2% DMSO (in water), put into an ultrasonic bath for 1 min and then shortly centrifuged. 10 µL of the resulting supernatant was mixed with 5 µL 100 fmol μL^{-1} Enolase digest (Waters, Eschborn, Germany) and acidified with 5 µL 1% formic acid (FA).

LC-MS Analysis: Liquid chromatography (LC) of tryptic peptides was performed on a NanoAQUITY UPLC system (Waters Corporation, Milford, MA) equipped with 75×10^{-6} M × 250 mm HSS-T3 C18 column (Waters Corporation). Mobile phase A was 0.1% (v/v) formic acid (FA) and 3% (v/v) dimethyl sulfoxide (DMSO) in water. Mobile phase B was 0.1% (v/v) FA and 3% (v/v) DMSO in acetonitrile (ACN). Peptides were separated running a gradient from 5 to 60% (v/v) mobile phase B at a flow rate of 300 nL min^{-1} over 60 min. The column was heated to 55 °C. MS analysis of eluting peptides was performed by data-independent acquisition (DIA) in MS^E. In brief, precursor ion information was collected in low-energy MS mode at a constant collision energy of 4 eV. Fragment ion information was obtained in the elevated energy scan applying drift-time specific collision energies. The spectral acquisition time in each mode was 0.6 s with a 0.05 s-interscan delay resulting in an overall cycle time of 1.3 s for the acquisition of one cycle of low and elevated energy data. [Glu1]-fibrinopeptide was used as lock mass at 100 fmol μL^{-1} and sampled every 30 s into the mass spectrometer via the reference sprayer of the NanoLockSpray source. All samples were analyzed in three technical replicates.

Data Processing and Label-Free Quantification: MS^E data processing and database search was performed using ProteinLynx Global Server (PLGS, ver. 3.0.2, Waters Corporation). The resulting proteins were searched against UniProt Human proteome database (UniProtKB release 2017_05, 20 201 entries) supplemented with a list of common contaminants. The database search was specified by trypsin as enzyme for digestion and peptides with up to two missed cleavages were included. Furthermore, Carbamidomethyl cysteine was set as fixed modification and oxidized methionine as variable modification. False discovery rate (FDR) assessment for peptide and protein identification was done using the target-decoy strategy by searching a reverse database and was set to 0.01 for database search in PLGS.

Retention time alignment, exact mass retention time (EMRT), as well as normalization and filtering was performed in ISOQuant ver.1.8.[71,72] By using TOP3 quantification,[73] absolute in-sample amounts of proteins were calculated. Statistical analysis was done in Perseus,[74] by performing two-tailed, paired -tests and subsequent Benjamini-Hochberg correction.[75] Q-values < 0.05 were considered as significant.

Statement Regarding the Patient Data: Final clinical protocol, amendments, and informed consent documentation were approved by the Independent Ethics Committee (IEC) at the sites in Belgium and the Netherlands. Clinical studies were conducted in accordance with the ethical principles of the Declaration of Helsinki and are consistent with the International Council for Harmonisation (ICH) E6 Good Clinical Practice (GCP) guidelines and applicable national laws and regulatory requirements.

Patients provided their written informed consent to participate in the study after having been informed about the nature and purpose of the study, participation/termination conditions, and risks and benefits of treatment. Informed consent was obtained before the start of screening procedures from all patients.

Supporting Information

Supporting Information is available from the Wiley Online Library or from the author.

Acknowledgements

The authors acknowledge support of the DFG (SFB 1066, project Q1). Furthermore, Ruben Spohrer is thanked for help with LC-MS measurements, Silvia Rizzelli for purification of the Cyanin7 functionalized pHPMA NPs by HPLC, and Christine Rosenauer for help with dynamic light scattering measurements. Wolfgang Schupp and ConSenxuS are thanked for help regarding the AF4 set-up.

Conflict of Interest

The authors declare no conflict of interest.

Keywords

asymmetrical flow field-flow fractionation, drug delivery, micellar structures, protein corona

Received: December 25, 2019
Revised: March 4, 2020
Published online: April 6, 2020

[1] M. J. Vicent, H. Ringsdorf, R. Duncan, *Adv. Drug Delivery Rev.* **2009**, *61*, 1117.
[2] M. van Elk, B. P. Murphy, T. Eufrásio-da-Silva, D. P. O'Reilly, T. Vermonden, P. W. E. Hennink, G. P. Duffy, E. Ruiz-Hernández, *Int. J. Pharm.* **2016**, *515*, 132.

© 2020 The Authors. Published by WILEY-VCH Verlag GmbH & Co. KGaA, Weinheim

[3] J. Shi, P. W. Kantoff, R. Wooster, O. C. Farokhzad, *Nat. Rev. Cancer* **2017**, *17*, 20.
[4] E. Blanco, H. Shen, M. Ferrari, *Nat. Biotechnol.* **2015**, *33*, 941.
[5] B. Sahoo, M. Goswami, S. Nag, S. Maiti, *Chem. Phys. Lett.* **2007**, *445*, 217.
[6] T. Cedervall, I. Lynch, S. Lindman, T. Berggård, E. Thulin, H. Nilsson, K. A. Dawson, S. Linse, *Proc. Natl. Acad. Sci. USA* **2007**, *104*, 2050.
[7] R. García-Álvarez, M. Hadjidemetriou, A. Sánchez-Iglesias, L. M. Liz-Marzán, K. Kostarelos, *Nanoscale* **2018**, *10*, 1256.
[8] N. Bertrand, P. Grenier, M. Mahmoudi, E. M. Lima, E. A. Appel, F. Dormont, J. M. Lim, R. Karnik, R. Langer, O. C. Farokhzad, *Nat. Commun.* **2017**, *8*, 777.
[9] A. Hilla, C. K. Paynea, *RSC Adv.* **2010**, *8*, 4017.
[10] S. Ritz, S. Scho, N. Kotman, G. Baier, A. Musyanovych, J. Kuharev, K. Landfester, H. Schild, O. Jahn, S. Tenzer, V. Maila, *Biomacromolecules* **2015**, *16*, 1311.
[11] J. Wang, U. B. Jensen, G. V Jensen, S. Shipovskov, V. S. Balakrishnan, D. Otzen, J. S. Pedersen, F. Besenbacher, D. S. Sutherland, *Nano Lett.* **2011**, *11*, 4985.
[12] M. C. L. Giudice, L. M. Herda, E. Polo, K. A. Dawson, *Nat. Commun.* **2016**, *7*, 1.
[13] T. Miclăuş, C. Beer, J. Chevallier, C. Scavenius, V. E. Bochenkov, J. J. Enghild, D. S. Sutherland, *Nat. Commun.* **2016**, *7*, 11770.
[14] L. Wang, J. Li, J. Pan, X. Jiang, Y. Ji, Y. Li, Y. Qu, Y. Zhao, X. Wu, C. Chen, *J. Am. Chem. Soc.* **2013**, *135*, 17359.
[15] A. Salvati, A. S. Pitek, M. P. Monopoli, K. Prapainop, F. B. Bombelli, D. R. Hristov, P. M. Kelly, C. Åberg, E. Mahon, K. A. Dawson, *Nat. Nanotechnol.* **2013**, *8*, 137.
[16] M. P. Monopoli, D. Walczyk, A. Campbell, G. Elia, I. Lynch, F. B. Bombelli, K. A. Dawson, *J. Am. Chem. Soc.* **2011**, *133*, 2525.
[17] M. Talelli, M. Barz, C. J. F. Rijcken, F. Kiessling, W. E. Hennink, T. Lammers, *Nano Today* **2015**, *10*, 93.
[18] D. Klepac, S. Petrova, P. Chytil, D. A. Weitz, S. K. Filippov, *Nanoscale* **2018**, *10*, 6194.
[19] C. Weber, M. Voigt, J. Simon, A. Danner, H. Frey, V. Mailänder, M. Helm, S. Morsbach, K. Landfester, *Biomacromolecules* **2019**, *20*, 2989.
[20] G. Caracciolo, *Nanoscale* **2018**, *10*, 4167.
[21] Q. Hu, C. J. Rijcken, R. Bansal, W. E. Hennink, G. Storm, J. Prakash, *Biomaterials* **2015**, *53*, 370.
[22] I. Pötsch, D. Baier, B. K. Keppler, W. Berger, in *Metal-Based Anticancer Agents* (Eds: A. Casini, A. Vessières, S. M. Meier-Menches), The Royal Society Of Chemistry, London **2019**, p. 308.
[23] D. Di Silvio, N. Rigby, B. Bajka, A. Mayes, A. Mackie, F. Baldelli Bombelli, *Nanoscale* **2015**, *7*, 11980.
[24] D. Docter, U. Distler, W. Storck, J. Kuharev, D. Wünsch, A. Hahlbrock, S. K. Knauer, S. Tenzer, R. H. Stauber, *Nat. Protoc.* **2014**, *9*, 2030.
[25] M. Hadjidemetriou, Z. Al-Ahmady, M. Mazza, R. F. Collins, K. Dawson, K. Kostarelos, *ACS Nano* **2015**, *9*, 8142.
[26] C. Weber, J. Simon, V. Mailänder, S. Morsbach, K. Landfester, *Acta Biomater.* **2018**, *76*, 217.
[27] J. C. Giddings, *Sep. Sci.* **1966**, *1*, 123.
[28] J. C. Giddings, *Science* **1993**, *260*, 1456.
[29] F. A. Messaud, R. D. Sanderson, J. R. Runyon, T. Otte, H. Pasch, S. K. R. Williams, *Prog. Polym. Sci.* **2009**, *34*, 351.
[30] J. Gigault, J. M. Pettibone, C. Schmitt, V. A. Hackley, *Anal. Chim. Acta* **2014**, *809*, 9.
[31] C. Weber, S. Morsbach, K. Landfester, *Angew. Chem., Int. Ed.* **2019**, *58*, 12787.
[32] Q. Hu, C. J. F. Rijcken, E. Van Gaal, P. Brundel, H. Kostkova, T. Etrych, B. Weber, M. Barz, F. Kiessling, J. Prakash, G. Storm, W. E. Hennink, T. Lammers, *J. Controlled Release* **2016**, *244*, 314.
[33] M. Barz, F. K. Wolf, F. Canal, K. Koynov, M. J. Vicent, H. Frey, R. Zentel, *Macromol. Rapid Commun.* **2010**, *31*, 1492.
[34] P. Chytil, E. Koziolová, T. Etrych, K. Ulbrich, *Macromol. Biosci.* **2018**, *18*, 1700209.
[35] D. Huesmann, A. Sevenich, B. Weber, M. Barz, *Polymer* **2015**, *67*, 240.
[36] B. Weber, A. Birke, K. Fischer, M. Schmidt, M. Barz, *Macromolecules* **2018**, *51*, 2653.
[37] Y. C. Barenholz, *J. Controlled Release* **2012**, *160*, 117.
[38] P. A. Vasey, S. B. Kaye, R. Morrison, C. Twelves, P. Wilson, R. Duncan, A. H. Thomson, L. S. Murray, T. E. Hilditch, T. Murray, S. Burtles, D. Fraier, E. Frigerio, *Clin. Cancer Res.* **1999**, *5*, 83.
[39] G. Settanni, T. Schäfer, C. Muhl, M. Barz, F. Schmid, *Comput. Struct. Biotechnol. J* **2018**, *16*, 543.
[40] S. Schöttler, K. Landfester, V. Mailänder, *Angew. Chem., Int. Ed.* **2016**, *55*, 8806.
[41] V. Hong Nguyen, B.-J. Lee, *Int. J. Nanomed.* **2017**, *12*, 3137.
[42] I. Negwer, A. Best, M. Schinnerer, O. Schäfer, L. Capeloa, M. Wagner, M. Schmidt, V. Mailänder, M. Helm, M. Barz, H. Butt, K. Koynov, *Nat. Commun.* **2018**, *9*, 5306.
[43] E. Ostuni, R. G. Chapman, R. E. Holmlin, S. Takayama, G. M. Whitesides, *Langmuir* **2001**, *17*, 5605.
[44] B. Weber, A. Birke, K. Fischer, M. Schmidt, M. Barz, *Macromolecules* **2018**, *51*, 2653.
[45] T. Lammers, R. Kühnlein, M. Kissel, V. Subr, T. Etrych, R. Pola, M. Pechar, K. Ulbrich, G. Storm, P. Huber, P. Peschke, *J. Controlled Release* **2005**, *110*, 103.
[46] C. Zhao, L. Li, J. Zheng, *Langmuir* **2010**, *26*, 17375.
[47] T. Schäfer, C. Muhl, M. Barz, F. Schmid, G. Settanni, in *High Performance Computing Science and Engineering'18* (Es: W. Nagel, D. Kröner, M. Resch), Springer, Cham **2019**, pp. 63–74.
[48] S. Kramer, K. O. Kim, R. Zentel, *Macromol. Chem. Phys.* **2017**, *218*, 1700113.
[49] C. Hörtz, A. Birke, L. Kaps, S. Decker, E. Wächtersbach, K. Fischer, D. Schuppan, M. Barz, M. Schmidt, *Macromolecules* **2015**, *48*, 2074.
[50] S. E. Mcneil, *Characterization of Nanoparticles Intended for Drug Delivery* (Ed: S. E. McNeil), Springer, Berlin **2011**.
[51] C. L. Braal, P. de Bruijn, F. Atrafi, M. van Geijn, C. J. F. Rijcken, R. H. J. Mathijssen, S. L. W. Koolen, *J. Pharm. Biomed. Anal.* **2018**, *161*, 168.
[52] F. Atrafi, H. Dumez, R. H. J. Mathijssen, C. W. Menke, J. Costermans, C. J. F. Rijcken, R. Hanssen, F. Eskens, P. Schöffski, *J. Clin. Oncol.* **2019**, *37*, 3026.
[53] A. Musyanovych, V. Fetz, S. Tenzer, D. Docter, R. Hecht, F. Schlenk, D. Fischer, K. Kiouptsi, C. Reinhardt, M. Maskos, S. K. Knauer, K. Landfester, R. H. Stauber, *Nat. Nanotechnol.* **2013**, *8*, 772.
[54] A. Lilia, G. Caruso, C. Cavaliere, A. Riccioli, S. Palchetti, A. Lagana, *Langmuir* **2013**, *29*, 6485.
[55] K. Rausch, A. Reuter, K. Fischer, M. Schmidt, *Biomacromolecules* **2010**, *11*, 2836.
[56] F. Caputo, A. Arnould, M. Bacia, W. L. Ling, E. Rustique, I. Texier, A. P. Mello, A.-C. Couffin, *Mol. Pharmaceutics* **2019**, *16*, 756.
[57] R. F. Schmidt, F. Lang, G. Thews, *Physiologie des Menschen*, Springer, Berlin **2007**.
[58] M. Chevallet, S. Luche, T. Rabilloud, *Nat. Protoc.* **2006**, *1*, 1852.
[59] M. Sielaff, J. Kuharev, T. Bohn, J. Hahlbrock, T. Bopp, S. Tenzer, U. Distler, *J. Proteome Res.* **2017**, *16*, 4060.
[60] M. Hadjidemetriou, S. McAdam, G. Garner, C. Thackeray, D. Knight, D. Smith, Z. Al-Ahmady, M. Mazza, J. Rogan, A. Clamp, K. Kostarelos, *Adv. Mater.* **2019**, *31*, 1803335.
[61] K. P. García, K. Zarschler, L. Barbaro, J. A. Barreto, W. O. Malley, L. Spiccia, H. Stephan, B. Graham, *Small* **2014**, *10*, 2516.
[62] D. F. Moyano, K. Saha, G. Prakash, B. Yan, H. Kong, M. Yazdani, V. M. Rotello, *ACS Nano* **2014**, *8*, 6748.

© 2020 The Authors. Published by WILEY-VCH Verlag GmbH & Co. KGaA, Weinheim

[63] M. Kokkinopoulou, J. Simon, K. Landfester, V. Mailänder, I. Lieberwirth, *Nanoscale* **2017**, *9*, 8858.
[64] L. Nuhn, E. Bolli, S. Massa, I. Vandenberghe, K. Movahedi, B. Devreese, J. A. Van Ginderachter, B. G. De Geest, *Bioconjugate Chem.* **2018**, *29*, 2394.
[65] L. Nuhn, L. Kaps, M. Diken, D. Schuppan, R. Zentel, *Macromol. Rapid Commun.* **2016**, *37*, 924.
[66] S. Kramer, D. Svatunek, I. Alberg, B. Gräfen, S. Schmitt, L. Braun, A. H. A. M. Van Onzen, R. Rossin, K. Koynov, H. Mikula, R. Zentel, *Biomacromolecules* **2019**, *20*, 3786.
[67] M. Marioli, W. T. Kok, *Anal. Bioanal. Chem.* **2019**, *411*, 2327.
[68] J. Tattersall, *Contrib. Nephrol.* **2007**, *158*, 201.
[69] U. K. Laemmli, *Nature* **1970**, *227*, 680.
[70] K. Mohr, M. Sommer, G. Baier, S. Schöttler, P. Okwieka, S. Tenzer, K. Landfester, V. Mailänder, M. Schmidt, R. G. Meyer, *J. Nanomed. Nanotechnol.* **2014**, *05*, 1000193.
[71] U. Distler, J. Kuharev, P. Navarro, S. Tenzer, *Nat. Protoc.* **2016**, *11*, 795.
[72] U. Distler, J. Kuharev, P. Navarro, Y. Levin, H. Schild, S. Tenzer, *Nat. Methods* **2014**, *11*, 167.
[73] J. C. Silva, M. V. Gorenstein, G.-Z. Li, J. P. C. Vissers, S. J. Geromanos, *Mol. Cell. Proteomics* **2006**, *5*, 144.
[74] S. Tyanova, J. Cox, *Methods Mol. Biol.* **2018**, *1711*, 133.
[75] Y. Benjamini, Y. Hochberg, *J. R Statistical Soc., Ser. B* **1995**, *57*, 289.

© 2020 The Authors. Published by WILEY-VCH Verlag GmbH & Co. KGaA, Weinheim